Electron paramagnetic resonance approaches to study biologically relevant reactions: examples from amyloid aggregation to enzymes

Passerini, L.

Chapter 1.
Introduction

Electron Paramagnetic Resonance (EPR), also known as Electron Spin Resonance (ESR), is a powerful technique to study materials with unpaired electrons. It was first observed by the Soviet physicist Yevgeny Zavoisky in 1944 [1, 2], and since then has become an essential tool for probing the electronic and structural properties of paramagnetic systems.

EPR is a magnetic resonance spectroscopy particularly valuable for studying paramagnetic ions, organic radicals, transition metal complexes and biological macromolecules. Since its discovery, EPR rapidly expanded its applications and is now well-established across diverse fields such as solid state physics, biochemistry, chemical catalysis, environmental sciences, and many more.

A typical commercial EPR spectrometer consists of a magnet, microwave resonator, controlling console, and microwave components, that are necessary for excitation of the sample and detection of the signal. The information obtained from the sample depends on the field strength and microwave radiation frequency, as measurements at different fields and frequencies can highlight distinct aspects of the electronic structure. For the studies shown in this thesis, both a commercial and a homebuilt spectrometer [3] were used, that are shown in figure 1.

In this thesis, the goal is to explore EPR approaches to improve the study of biochemically relevant problems, and to learn about the mechanisms of biochemical reactions. One important problem is amyloid aggregation, where difficult-to-study intermediates are considered active in neurodegenerative diseases. In chapter 3 we explore in-depth how EPR can contribute to this research. In the course of the investigation related to chapter 3, we encountered a problem that has been around for at least four decades of spin-labelling EPR, which we were able to solve in chapter 2. In all physiological events involving proteins that catalyze chemical reactions, so called enzymes, efficiency and specificity is determined by the reaction mechanism. Chapter 4 shows how a new method relying on very-high field EPR enables to determine a short-lived intermediate of such a reaction. In chapter 5, a model system is studied that targets distances in multi-spin systems expanding the technique to Cu(II) spins. Multispin interactions in Cu(II) and related spin systems are important in many biological systems.

In this introductory chapter, the fundamental concepts of EPR are presented, along with the necessary information to understand the scientific studies in chapters 2 through 5. The background of EPR is described in several monographies [4-6]. Here specifically [6] is used, in addition to the references mentioned for specific points.

Figure 1. Spectrometer used for electron paramagnetic resonance (EPR). Left: Bruker Elexsys E580 9 GHz EPR spectrometer, operating magnetic field 0-0.5 T. Right: Homebuilt 275 GHz EPR spectrometer, operating magnetic field 0-11 T. Here the magnet is a superconducting coil immersed in liquid helium.

1.1 The Spin Hamiltonian

The information obtained with EPR can be described by the spin Hamiltonian, which represents the total energy of the spin-system and provides the theoretical support for interpreting EPR spectra. The spin Hamiltonian relevant to this thesis for a two electron- one nucleus system can be expressed as:

$$\hat{H} = \sum_{n=1,2}(\mu_B \boldsymbol{g}\boldsymbol{B_0}\widehat{\boldsymbol{S}_n} + \hat{\boldsymbol{I}}\boldsymbol{A}_n\widehat{\boldsymbol{S}_n}) + \widehat{\boldsymbol{S}_1}\boldsymbol{D}\widehat{\boldsymbol{S}_2} + J\widehat{\boldsymbol{S}_1}\widehat{\boldsymbol{S}_2} \quad (1)$$

Here, $\mu_B \boldsymbol{g}\boldsymbol{B_0}\widehat{\boldsymbol{S}_n}$ is the electron Zeeman interaction between the unpaired electron and the applied magnetic field $\mathbf{B_0}$, with $\hat{\boldsymbol{S}}$, the electron spin vector operator and **g** the g-tensor. $\hat{\boldsymbol{I}}\boldsymbol{A}_n\widehat{\boldsymbol{S}_n}$ is the hyperfine interaction between the unpaired electrons and a coupled magnetic nucleus, with $\hat{\boldsymbol{I}}$, the nuclear spin vector operator and $\boldsymbol{A}_n$ the hyperfine tensors. $\widehat{\boldsymbol{S}_1}\boldsymbol{D}\widehat{\boldsymbol{S}_2}$ and $J\widehat{\boldsymbol{S}_1}\widehat{\boldsymbol{S}_2}$ are the dipole-dipole and exchange interaction, respectively, between the unpaired electron and other nearby unpaired electrons. Here, **D** is the dipolar tensor and J the isotropic exchange interaction. The origin of these terms and their impact on the EPR spectrum is discussed in the following sub-chapters. It is convenient to describe these energy terms in frequency units. In this thesis, the hyperfine interaction **A**, dipole-dipole interaction **D**, and exchange interaction J will be given in units of Hz.

1.2 Continuous wave EPR and the Electron Zeeman Interaction

This section focuses on continuous wave EPR (CW-EPR), where the sample is continuously irradiated with microwaves while the field is varied. The foundation of EPR spectroscopy lies in the interaction of the magnetic dipole moment of the electron spin with an applied static magnetic field B_0. During a CW-EPR experiment, the magnetic field lifts the degenerancy between the spin-energy levels of the unpaired electron (spin quantum number $S = 1/2$, magnetic quantum number $m_s = \pm 1/2$ for an isolated electron) while the sample is irradiated with microwaves (figure 2). The microwave-radiation frequency is kept constant during the experiment. This allows to place the sample in a microwave resonator, whose dimension is tuned to the microwave-radiation wavelength. If the energy difference between the spin states matches the energy of the microwave radiation, a transition occurs, producing an EPR signal. In EPR, the selection rule for allowed transition is $\Delta m_s = \pm 1$, meaning that the magnetic quantum number m_s can only change by one unit. The EPR spectrum is usually displayed as the first derivative of an absorption signal due to the use of lock-in detection, see figure 2.

A fundamental parameter in EPR is the g-factor, which determines the proportionality between the magnetic field strength and the energy of the electron spin transition:

$$\hat{H} = \mu_B \boldsymbol{g} \boldsymbol{B_0} \hat{\boldsymbol{S}} \tag{2}$$

where $\hat{\boldsymbol{S}}$ is the electron spin vector operator, $\mathbf{g}$ the g-tensor, μ_B is the Bohr magneton, and $\boldsymbol{B_0}$ is the static magnetic field vector. The resonance condition for a free electron is given by:

$$h\nu = \mu_B g_e B_0 \tag{3}$$

where h is the Planck constant and ν is the microwave frequency. For a free electron, the g-value (g_e) is 2.0023. However, in atoms and molecules deviations arise that depend on the spin-orbit coupling and chemical environment. These effects cause the g-factor to deviate from g_e and to become anisotropic, meaning it varies depending on the molecule's orientation relative to the magnetic field. This anisotropy is expressed as the g-tensor $\mathbf{g}$. The principal values of $\mathbf{g}$ are [g_{xx} g_{yy} g_{zz}], can be resolved in solid-state EPR and single-crystal studies.

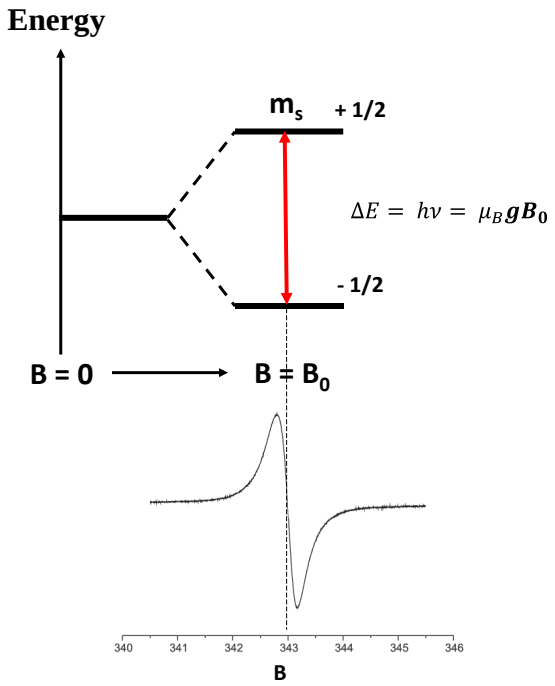

Figure 2. When the microwave-radiation frequency matches the energy difference between spin energy levels, a transition occurs. The EPR spectrum is depicted as first derivative of an absorption spectrum.

1.3 The Hyperfine Interaction

The hyperfine interaction is the interaction of the electron spin with the magnetic moment of a coupled nucleus. The degenerancy of the spin-energy levels of the nuclei is lifted in the presence of a magnetic field by the nuclear Zeeman interaction, generally weaker than the electron Zeeman interaction. The coupling of an unpaired electron with a nucleus with spin quantum number I, is given by the second term in the equation:

$$\hat{H} = \mu_B \boldsymbol{g} \boldsymbol{B_0} \hat{\boldsymbol{S}} + \hat{\boldsymbol{I}} \boldsymbol{A} \hat{\boldsymbol{S}} \quad (4)$$

where **A** is the hyperfine tensor with principal values [A_{xx} A_{yy} A_{zz}] and $\hat{\boldsymbol{I}}$ is the nuclear spin vector operator. The hyperfine interaction manifests in the EPR spectrum as a splitting of the signal in $(2I+1)$-lines. In figure 3, the energy-level scheme for an electron coupled to a ^{14}N ($I=1$) nucleus is shown, which results in the three transitions shown in red. In chapter 4 and 5, systems with copper ions are studied. The Cu(II) nucleus has nuclear spin quantum number $I=3/2$, and the signal is split into four lines. In this thesis, chapter 2 and 3 focus on measurements on liquid samples, where the anisotropy of **g**- and **A**-tensors is averaged by the rapid tumbling of the molecule in solution. For very fast motion, the observed g and A-values are $g_{iso}=\frac{g_{xx}+g_{yy}+g_{zz}}{3}$ and $A_{iso}=\frac{A_{xx}+A_{yy}+A_{zz}}{3}$. In chapter 4 and 5, samples in frozen solutions are measured. In this case, a powder pattern is observed, due to the statistical distribution of all possible orientations of the molecules in the magnetic field, which has characteristic features of the principal values of the tensors.

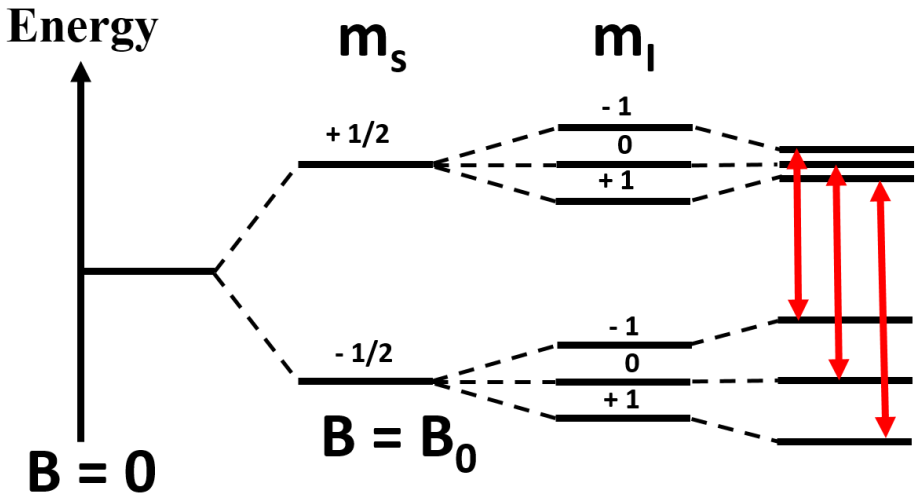

Figure 3. Energy level scheme for an electron coupled with a ^{14}N nucleus, I = 1. The magnetic field induces a splitting of the electron spin energy levels by electron Zeeman interaction, and a splitting between nuclear spin energy levels by nuclear Zeeman interaction. The hyperfine interaction results in 2I+1 transitions, shown in the figure as red arrows.

1.4 Dipole-Dipole Interaction

The electron-electron-dipole-dipole interaction in EPR arises when two unpaired electrons are sufficiently close that each one's magnetic field influences the other. This interaction depends on the distance between the two spins and on the orientation of the vector connecting them with respect to the field vector (see sub-section 1.8).
The spin Hamiltonian for a system with two interacting spins, describing the combined effects of the electron Zeeman, hyperfine, and dipole-dipole interactions, is expressed as:

$$\hat{H} = \sum_{n=1,2}(\mu_B \boldsymbol{g}\boldsymbol{B_0}\widehat{\boldsymbol{S}_n} + \hat{\boldsymbol{I}}\boldsymbol{A}_n\widehat{\boldsymbol{S}_n}) + \widehat{\boldsymbol{S}_1}\boldsymbol{D}\widehat{\boldsymbol{S}_2} \quad (5)$$

The dipole-dipole interaction is given by the **D**-tensor. Adopting the point-dipole approximation, the **D**-tensor has axial symmetry and is traceless ($D_{xx} + D_{yy} + D_{zz} = 0$).
In CW-EPR spectra, the dipole-dipole interaction can broaden or split signals depending on its magnitude and orientation relative to the magnetic field. In pulsed EPR experiments, such as those performed in chapter 5, the distance dependence of this interaction is used to extract inter-spin, intramolecular distances. The relation between **D** and the distance between the two spins is discussed in subchapter 1.8.

1.5 Exchange Interaction

The exchange interaction arises in systems containing two or more unpaired electrons and is described by $H_{exchange} = J\widehat{\boldsymbol{S}_1}\widehat{\boldsymbol{S}_2}$ with J being the isotropic exchange coupling constant. Unlike the dipole-dipole interaction, which depends on the spatial separation and orientation of spins, the exchange interaction is a quantum-mechanical effect related to the overlap of electron-spin wavefunctions [7].

In this thesis the exchange coupling interaction is relevant in chapter 2 and in chapter 4. In chapter 2, two exchange coupled nitroxides (see figure 4) are measured at room temperature. In this situation, the relative magnitude of J with respect to the isotropic hyperfine interaction A_{iso} of the electron spin with the nitrogen nuclei is the main factor to determine the EPR spectral shape. To use the same words as in [7], for strong exchange

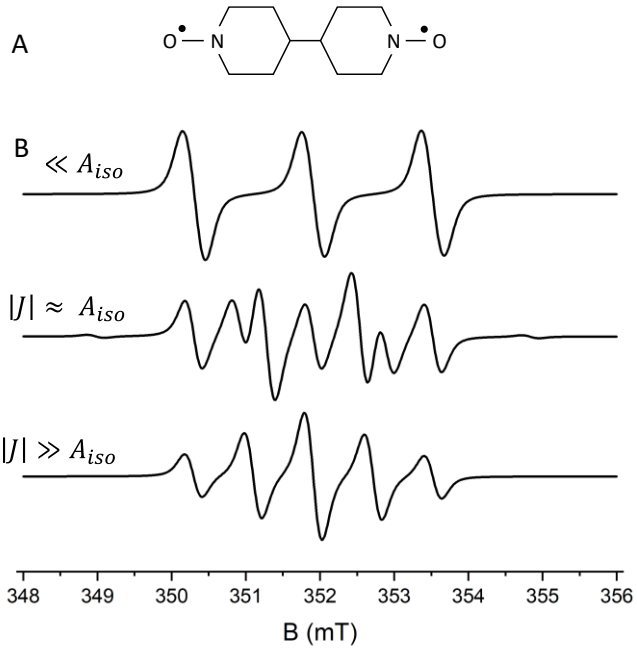

Figure 4. Exchange coupling in nitroxide biradicals. A) Example of a nitroxide biradical. The unpaired electrons are coupled to the ^{14}N nuclei. B) Simulated EPR spectra for different values of J, for A_{iso} = 45 MHz. B): top spectrum: for small magnitude of J, the spectrum is the same as a nitroxide mono-radical. Bottom: for large magnitude of J with respect to A_{iso}, a five line spectrum appear, while complicated line shapes appear when the values of J and A_{iso} are of similar magnitude.

coupling ($J>>A_{iso}$), "strong exchange results in the electron interacting equally with both ^{14}N nuclei, but for half of the time", resulting in the five-line spectrum in figure 4B (bottom). For weak exchange ($J<<A_{iso}$) the spectrum will be the same as a single nitroxide radical, and relatively complicated spectral shapes are observed when J and A_{iso} are of similar magnitude. An extensive overview of exchange coupled nitroxide systems is given in [8].

In chapter 4, a protein is studied in which a Cu(II) ($3d^9$, $S = {}^1/_2$) ion is coupled to an organic radical ($S = {}^1/_2$). The two unpaired electrons are coupled into a triplet state, and this example illustrates how a multi frequency EPR approach aids to fully characterize the spin

Hamiltonian. In figure 5 the energy-level scheme, EPR transitions and EPR spectra for an exchange-coupled Cu(II)-radical system are given (J = -19 GHz), for 9 GHz and 275 GHz EPR. For clarity, the hyperfine coupling to the Cu nucleus is not included in the simulation. At 9 GHz (figure 5A) the energy separation between singlet and triplet state is larger than the

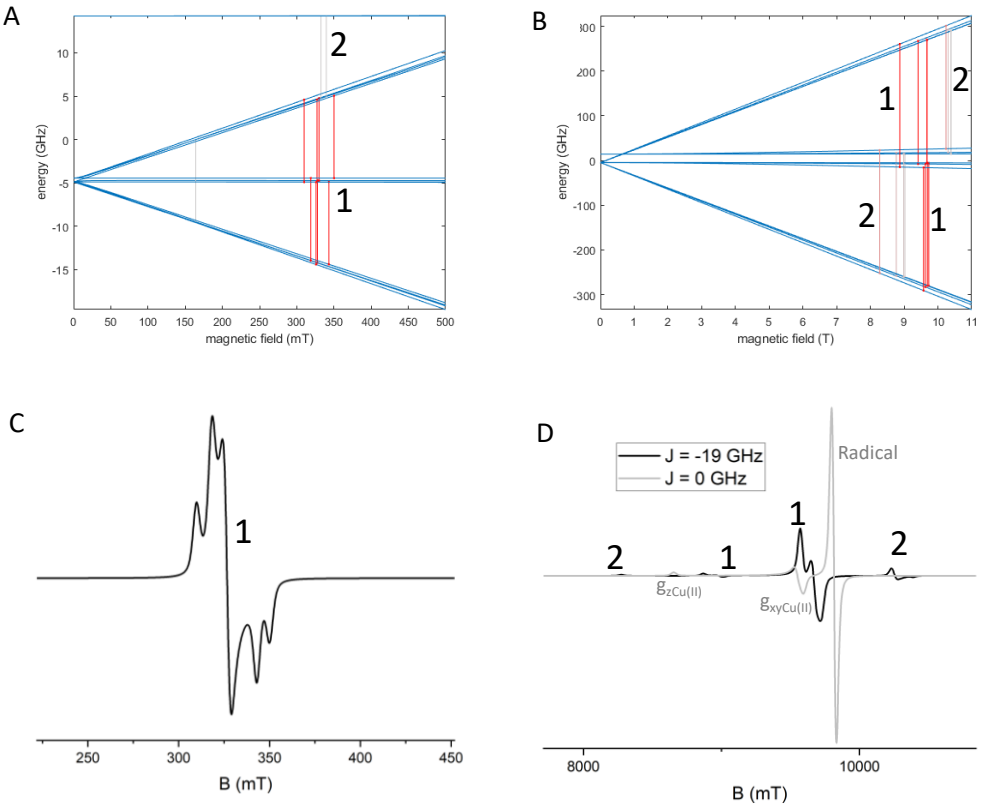

Figure 5. Effect of exchange coupling J on a coupled Cu(II)-organic radical system. The two unpaired electrons are coupled into a triplet ground state. A) Energy-level scheme for 9 GHz EPR. B) Energy-level scheme for 275 GHz EPR. C) 9 GHz EPR spectrum. D) 275 GHz EPR spectrum. Black: 275 GHz EPR for J = -19 GHz. Grey: 275 GHz EPR spectrum for J = 0 GHz. The spectrum is the one of a separated Cu(II) spectrum with axial symmetry (gx=gy≠gz) and an organic radical spectrum. In absence of magnetic field, the energy levels are separated into a triplet and a singlet ground state. These levels are mixed in the presence of a strong magnetic field. Transition 1: transition happening between the (original) triplet state sublevels. Transition 2: transition occurring between singlet and original triplet state. In the energy level scheme, the blue lines are the energy levels. The color of the transition lines indicates their probability: red: high, light grey: partially allowed

microwave quantum. Each triplet sublevel is split into four levels by the g-anisotropy, and the EPR spectrum has a complicated structure with six visible lines, and more lines hidden in the linewidth, but revealed in the energy levels scheme. In this condition, the magnitude of the exchange coupling is so large that values of |J| higher than 19 GHz would not affect the EPR spectrum further, as higher |J| would only introduce a larger separation of the triplet and singlet states, without affecting the transitions visible in the EPR spectrum. For this reason, the magnitude of J cannot be determined for such a system at 9 GHz EPR. The 275 GHz EPR energy level diagram is shown in figure 5B and the spectrum in figure 5D. In presence of a strong magnetic field, the triplet state is no longer a well-defined state as the energy levels undergo mixing. However, for simplicity, it is convenient to refer to them as "original triplet sublevels". It can be seen in figure 5C that transitions between these original triplet-sublevels and the singlet state are clearly visible in the 275 GHz EPR spectrum (transition 2 in figure 5B and 5D) whereas they do not appear in the 9 GHz EPR spectrum. The high-frequency spectrum is dominated by a signal split into two lines, situated between the transition of an isolated Cu(II) g_x and g_y resonance and an isolated organic radical, and a lower-intensity peak situated between the g_z of the Cu(II) and the radical (transitions labelled as 1). In this case the transitions (2) are diagnostic of the magnitude of the exchange coupling, which can be determined combining 9 and 275 GHz EPR. A multi-frequency EPR approach allows to fully characterize the spin Hamiltonian: It enables to determine the **D**-tensor principal values by 9 GHz EPR, and the J value by a combination of 9 and 275 GHz EPR.

1.6 EPR of Nitroxides and Site-directed-spin-labeling

Site-directed-spin-labeling (SDSL) is a technique that uses the attachment of spin labels to cysteine residues in proteins. In chapter 3, SDSL is used to study the aggregation of the intrinsically disordered protein α-Synuclein, a process that is linked to neurodegeneration (see below). In combination with site-directed mutagenesis, which allows to insert cysteine residues in selected protein sites while removing native unwanted ones, SDSL coupled with EPR allows to obtain site-specific information on biomolecules. The most commonly used spin labels are nitroxide radicals. The most well-known, MTSL ((1-Oxyl-2,2,5,5-tetramethylpyrroline-3-methyl) methanethiosulfonate), is shown in figure 6. In nitroxides, the unpaired electron spin interacts with the nitrogen (^{14}N, $I = 1$) nucleus, with an hyperfine coupling in the order of 100 MHz along the A_z direction and 10 MHz along A_x and A_y, which results in the characteristic splitting of the EPR signal into three lines. The EPR spectral shape of nitroxides at room temperature depends on their rotational correlation time τ_r (figure 6). The τ_r observed reflects the rotameric motion of the label and of the bonds connecting it to the protein backbone (figure 6B left). In specific circumstances, also the tumbling of the

molecule or the mobility of specific parts of the protein are influencing the spectral shape, especially when the molecular tumbling is faster than the rotameric motion of the label [9, 10] (figure 6B, right). In figure 6C, spectral simulations for different rotational correlation times show the relation between spectral shape and molecular motion. In the solid-state spectrum, figure 6C, the anisotropy of the A- and g-tensor is evident, while in liquid state the rapid tumbling of the free label in solution averages the anisotropy, resulting in the three-line spectrum for τ_r = 0.01 ns. When the label is attached to a protein, the tumbling will slow down, affecting the spectrum, because of the larger dimensions of the object. Site-specific structural and dynamical information in CW-EPR are obtained from the τ_r of the label. Changes in the spectral lineshape can give insights into interaction with partners, conformational changes, or environmental effects [11-14]. In chapter 3, SDSL coupled to CW-EPR is used to study the aggregation of the protein α-Synuclein, a process involved in Parkinson's disease. When in monomeric form, the protein tumbling in solution is fast, and results in a spectrum similar to the τ_r = 0.3 ns simulation in figure 6C. Inside aggregates, the motion is slower, and the spectrum looks like the τ_r = 7.94 ns simulation. By measuring changes in spectral shape over time, the aggregation process can be followed. When combined with pulsed EPR techniques, SDSL is an even more powerful method: if two labels are present within a nanometer range inside a protein, their distance can be measured using the EPR method described in subchapter 1.8.

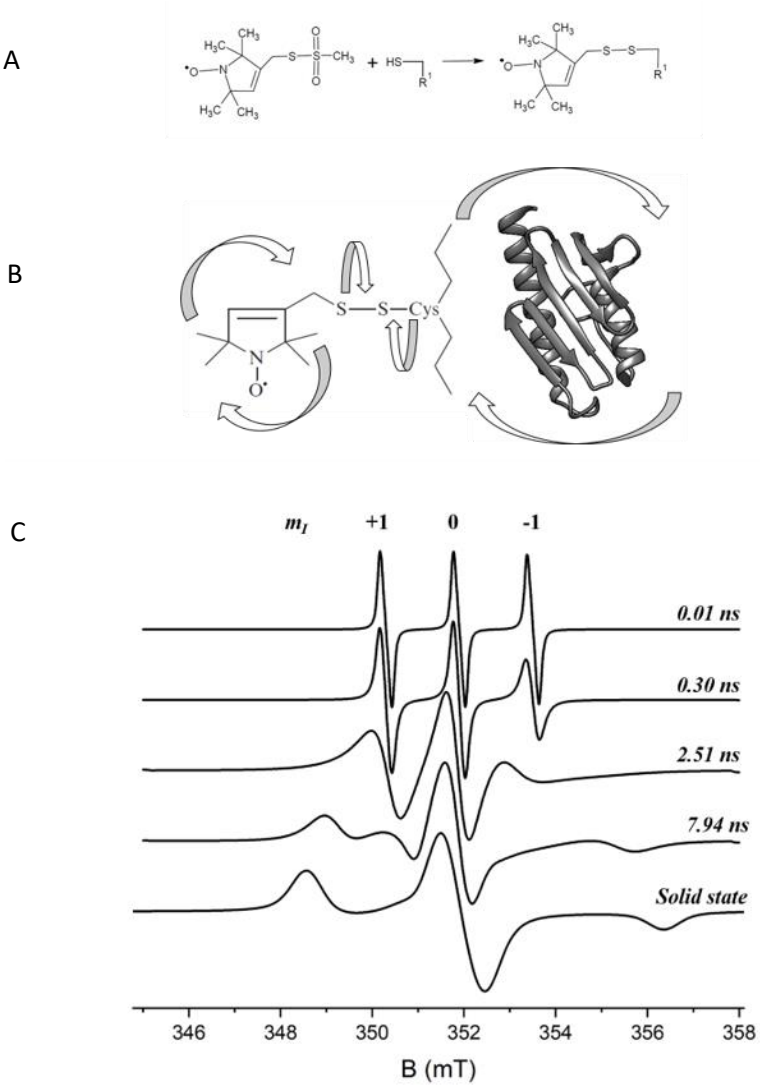

Figure 6. Site directed spin labeling (SDSL) and effect of spin label rotation on nitroxide EPR spectra. A) Reaction scheme of the attachment of MTSL spin label to a cysteine residue on a protein. B) The EPR spectrum will depend on the motion of the label, i.e. by the rotameric motion of the label (arrows indicating rotation of the bonds and of the proxyl ring) and by the molecular tumbling of the protein in solution (arrows around the protein structure). The protein shown in grey, Frataxin, is a small globular protein (14 KDa) and an increase in solution viscosity was necessary to slow the molecular tumbling and probe site-specific dynamics [10]. C) Simulated EPR spectra of a nitroxide spin label for different rotational correlation time.

1.7 Multifrequency EPR

By looking at the spin Hamiltonian (eq. 1), it is evident that only one term, the Zeeman interaction, depends on the field $\mathbf{B_0}$. By varying the magnetic field at which the experiment is performed – together with the operating frequency of the microwave radiation – different aspects of the spin Hamiltonian can be explored. For instance, the g-tensor anisotropy is better resolved at higher magnetic fields, due to the increased separation of energy levels. An example is illustrated in figure 7, where the solid state spectrum of a nitroxide is given at 9 and 275 GHz EPR. At 9 GHz EPR, the hyperfine coupling A_z dominates the spectrum, and the **g**-tensor is poorly resolved. At 275 GHz EPR, the **g**-tensor anisotropy can be accurately measured, and is dominating the spectral shape, while only the A_z component of the hyperfine is resolved. In chapter 4, a Cu(II) system is analyzed at different frequencies. Copper in the 9 GHz EPR solid-state spectrum (figure 8) appears as an axially symmetric spectrum (g_x and g_y not resolved). The hyperfine splitting with the Cu(II) nucleus into four

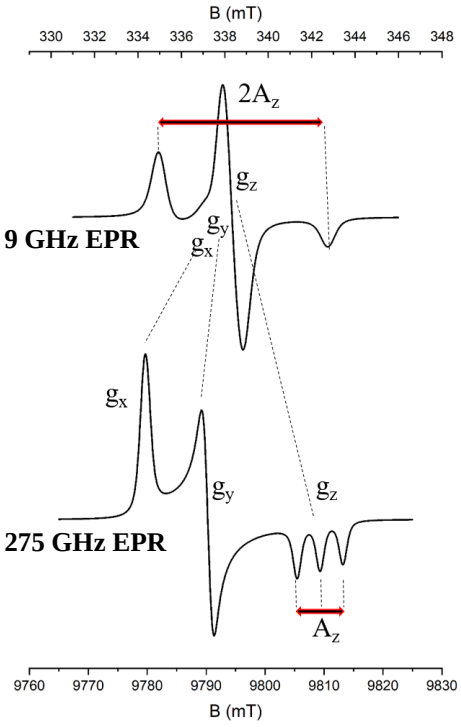

Figure 7 Examples of multifrequency EPR on a nitroxide system: the nitroxide spectrum at 9 GHz is dominated by the large A_z, and the g-tensor is poorly resolved. At 275 GHz, the g-tensor is well resolved.

lines ($I_{Cu} = {}^{3}/_{2}$) is resolved along the z-direction. At 275 GHz EPR small deviations from axial symmetry, i.e. small differences between g_x and g_y components, are resolved. At the same time, the hyperfine splitting A_z is hidden in the broader linewidth, and can't be accurately measured.

A combination of measurements at different frequencies offers unique insights into the electronic properties of complex systems and allows to fully evaluate their spin Hamiltonian parameters. This approach enhances the versatility of EPR, as multiple frequencies can also be applied to pulsed methods, allowing detailed characterization of paramagnetic systems.

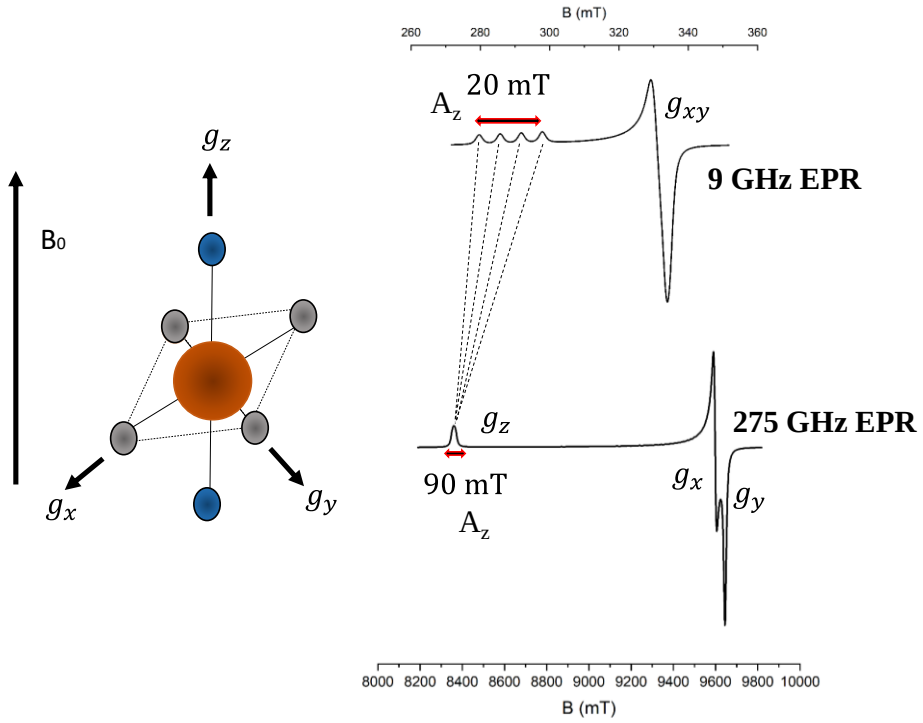

Figure 8 Example of multifrequency EPR on a Cu(II) complex. Right: EPR simulations show that in the 9 GHz EPR spectrum of a copper system with minor deviation from axial symmetry, the difference between g_x and g_y is not resolved, with $g_x \approx g_y$, and the A_z hyperfine splitting resolved along the g_z direction. At 275 GHz, the difference between g_x and g_y is resolved, but information on hyperfine coupling is masked by the linewidth. Left: structure scheme illustrating the copper center (orange) on which the unpaired electron is localized, coordinated in an octahedral geometry by the ligands (grey and blue spheres). The arrows indicate approximate g-tensor directions. The x and y coordination are nearly identical. Subtle deviations from axial symmetry, i.e. differences between g_x and g_y induced by slightly different coordination or tilting of the ligands, can only be resolved at high frequency EPR.

1.8 Double Electron Electron Resonance (DEER)

Double electron electron resonance spectroscopy is a pulsed EPR method designed to measure dipole-dipole interactions between unpaired electrons within a nanometer distance (typically 1.5-10 nm) [15]. From the dipole-dipole interaction, the distance between the spins can be extracted. This method is particularly powerful to obtain distance constraints in doubly spin-labelled proteins, providing insight into their structure and function. Due to fast relaxation times of the electron spins, DEER experiments are performed at cryogenic temperatures.

The pulse sequence used in chapter 5 for DEER spectroscopy is shown in figure 9. Microwaves are applied in pulses, whose length, power and timing depends on the specific applications and samples. A detailed description is provided in [16]. To describe DEER, here we follow the lines of [17]. The DEER technique is a double frequency experiment: the observer frequency is used to detect a signal from spin A, and the pump frequency will excite the second spin, B, that is coupled to A. During the experiment, the observer sequence is kept constant, while the timing of the pump pulse is varied. The resulting data (see figure 9) will consist of a time trace which shows the intensity of the signal detected for A as a function of pump pulse's position in the sequence.

The primary DEER data contains information about intramolecular interactions, and a background decay that depends on intermolecular interactions (figure 9B). After removal of the background decay, the form factor is obtained (figure 9C). In the form factor the modulation depth Δ depends on the amount of pumped B spins, while the modulations contain information about the dipole-dipole interactions. From the form factor, a distance distribution plot is derived, giving the population of spin-pair distances as a function of the distance (figure 9D).

After background correction, the signal amplitude as a function of time for i pumped spins B_i is given by:

$$f(t) = \prod_i^N \{1 - \lambda_i [1 - cos(\omega_{dd,i} t)]\} \quad (6)$$

where λ is the inversion efficiency of the pump pulse (how effectively the pump pulse inverts the B spins), with Δ = λ for two spin systems, and ω_{dd} is the electron-electron coupling frequency, which relates to the distance between the spins and their relative orientation:

$$\omega_{dd,i} = \left({}^{C_i}/_{r_i^3} \right) (1 - 3cos^2\theta_i) \quad (7)$$

Here, θ is the angle between the inter-spin vector and the magnetic field, r is the distance between the spins, and $C_i = \frac{\mu_0 g_1 g_2}{4\pi h}$, where μ_0 is the vacuum permeability, g_1 and g_2 are the g-factors of the spins, and h is the Planck's costant. From here, there are several methods to obtain distance distribution, used in chapter 5 are Tikhonov regularization, Gaussian fitting, and the neural networks based method DEERNet [18-20].

Complications arise in systems with more than two coupled spins. In figure 9 an example is given for a three spin system with spins A, B and C. In such systems, the signal from A will not just be modulated by the pairwise dipole-dipole interaction frequencies (ω_{AB} and ω_{AC}), but also by the sum and difference of those frequencies [21]. The form factor for the three-spin system is obtained by summing over all N possible observer spins:

$$F(t) = \frac{1}{N}\sum_{A=1}^{N}\prod_{A\neq B}^{N} f_{AB}(t) \tag{8}$$

Here, $f_{AB}(t) = 1 - \lambda_B(1 - \cos(\omega_{AB}t))$ is the dipolar evolution of an individual spin pair. Additional modulations in the form factor introduce artifacts in the distance distribution, referred to as ghost distances. Several methods have been developed to minimize these artifacts to obtain pure pairwise distances from multispin systems. On one hand, the problem can be solved experimentally: by adjusting the power of the pump pulse, it is possible to pump less spins, thereby reducing multispin effects. An effect similar is achieved by using paramagnetic species with broad, anisotropic spectra, where only a smaller fraction of the pumped spins can be excited. In [21] a method was developed to suppress multispin effects during data processing. This method relies on applying the scaling exponent 1/(N-1) to the multispin form factor, where N is the number of spins contributing to the signal. This method is called "power scaling". In [22] a method to count how many spins are contributing to the DEER signal was designed. It is based on the fact that the modulation depth Δ observed for multispin systems and the modulation depth λ of a two-spin reference have the following relation:

$$\Delta_N = 1 - (1 - \lambda)^{N-1} \tag{9}$$

With N being the number of spins. Particular care has to be taken: the multispin and the two-spin systems need to be similar systems (the same paramagnetic species) and measured under identical experimental conditions. A detailed description of DEER spectroscopy is given in [17].

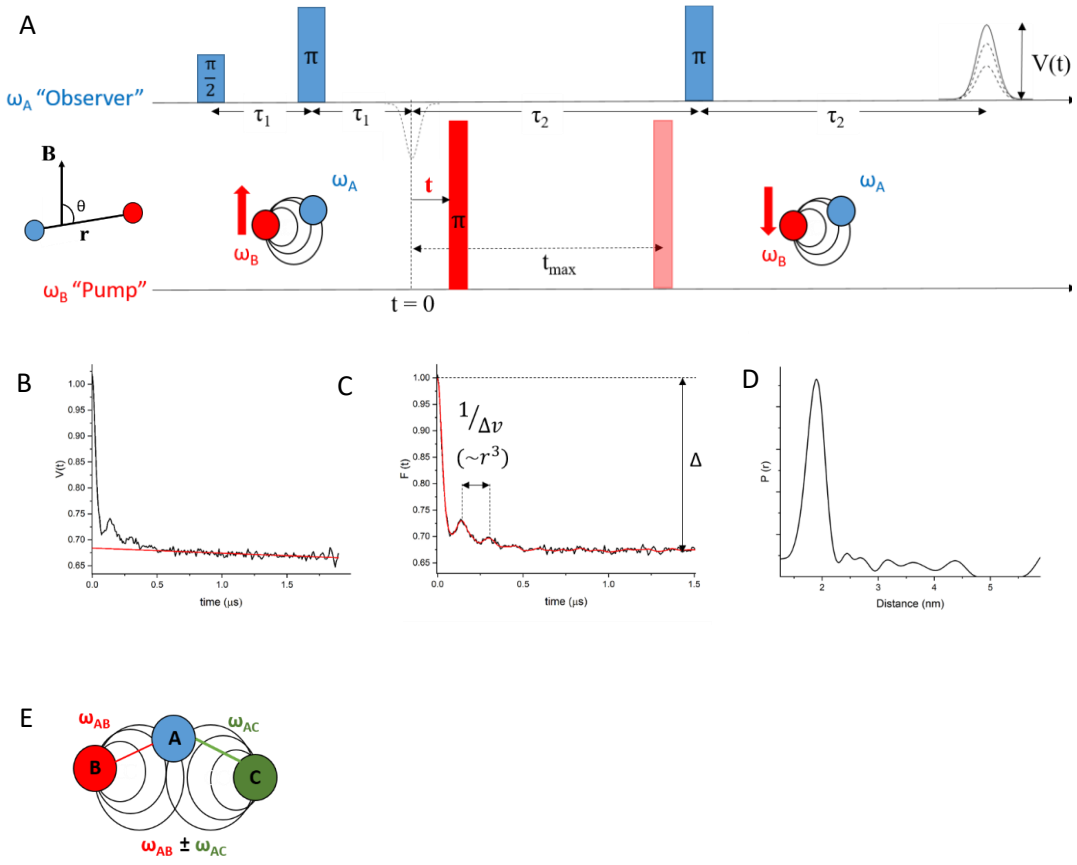

Figure 9. DEER spectroscopy. A) Pulse sequence. Blue: observer sequence. Red: pump sequence. Inset: in equation 7, θ is the angle between the field direction and the vector connecting the two spins. B) Primary data (black) and background decay (red). C) Form factor after background subtraction. F(t) contains information on number of spins (Δ) and the modulation contain information on dipolar interaction. D) Distance-distribution plot. E) In a three spin system, additional modulation come from sum and difference frequencies, producing artifacts in the distance distribution.

1.9 Overview of the thesis chapters

This thesis explores application of EPR methods on diverse systems. Chapter 2 examines how MTSL, the spin label (figure 6A) used to label and probe specific sites in bio-molecules, is forming dimers in aqueous solution. The dimerization process is limiting the efficiency of the labelling reaction. In chapter 2 the dimerization is studied in detail and a proposal is made for the dimer structure and the dimerization reaction mechanism. In chapter 3, EPR is used in combination with site-directed-spin-labeling (SDSL), to investigate the aggregation of the intrinsically disordered protein α-Synuclein. α-Synuclein aggregation is a process involved in Parkinson's disease. The goal is to develop an EPR method to identify the different species formed during the aggregation process, with a focus on the aggregation intermediates, the toxic species involved in the neurodegeneration [23]. Chapter 4 uses a multifrequency EPR approach to characterize a short lived intermediate formed in the reaction between Small LACcase (SLAC), an algae-derived enzyme, with oxygen. The protein SLAC is an interesting enzyme for industrial applications and characterization of its active site is crucial for bioengineering and development of biomimetic catalysts [24]. Finally, in chapter 5, a pulsed EPR method is applied to derive structural information from supramolecular, self-assembled metallo-organic complexes, giving a first example of the application of dipolar EPR spectroscopy to systems containing multiple Cu(II) ions.

1.10 References

[1] Zavoisky Y., Paramagnetic Absorption in Perpendicular and Parallel Fields for Salts, Solutions and Metals, Kazan State University., 1944.

[2] Zavoisky Y., Spin-magnetic resonance in paramagnetics, Fizicheskiĭ Zhurnal 9 (1945) 211-245.

[3] H. Blok, J.A.J.M. Disselhorst, S.B. Orlinskii, J. Schmidt, A continuous-wave and pulsed electron spin resonance spectrometer operating at 275GHz, Journal of Magnetic Resonance 166(1) (2004) 92-99.

[4] J.R. Bolton, J.A. Weil, Electron Paramagnetic Resonance - Elementary Theory and Practical Applications, John Wiley & Sons2007.

[5] N.M. Atherton, Electron Spin Resonance: Theory and Applications, Ellis Horwood1993.

[6] D. Goldfarb, S. Stoll, EPR spectroscopy. Fundamentals and Methods (Book), John Wiley & Sons, 2018.

[7] D. Goldfarb, S. Stoll, E.J.L. McInnes, D. Collison, Chapter 4, EPR Interactions - Coupled Spins, EPR spectroscopy. Fundamentals and Methods (Book), John Wiley & Sons, 2018.

[8] S.S. Eaton, L.B. Woodcock, G.R. Eaton, Continuous wave electron paramagnetic resonance of nitroxide biradicals in fluid solution, Concepts Magn Reson Part A Bridg Educ Res 47A(2) (2018).

[9] C.J. López, M.R. Fleissner, Z. Guo, A.K. Kusnetzow, W.L. Hubbell, Osmolyte perturbation reveals conformational equilibria in spin-labeled proteins, Protein Science 18(8) (2009) 1637-1652.

[10] D. Doni, L. Passerini, G. Audran, S.R.A. Marque, M. Schulz, J. Santos, P. Costantini, M. Bortolus, D. Carbonera, Effects of Fe2+/Fe3+ Binding to Human Frataxin and Its D122Y Variant, as Revealed by Site-Directed Spin Labeling (SDSL) EPR Complemented by Fluorescence and Circular Dichroism Spectroscopies, International Journal of Molecular Sciences, 2020.

[11] A. Czogalla, A. Pieciul A Fau - Jezierski, A.F. Jezierski A Fau - Sikorski, A.F. Sikorski, Attaching a spin to a protein -- site-directed spin labeling in structural biology, (0001-527X (Print)).

[12] P.G. Fajer, Electron Spin Resonance Spectroscopy Labeling in Peptide and Protein Analysis, Encyclopedia of Analytical Chemistry 2006.

[13] C.S. Klug, J.B. Feix, Methods and Applications of Site-Directed Spin Labeling EPR Spectroscopy, Methods in Cell Biology, Academic Press2008, pp. 617-658.

[14] M.R. Fleissner, D. Cascio, W.L. Hubbell, Structural origin of weakly ordered nitroxide motion in spin-labeled proteins, Protein Science 18(5) (2009) 893-908.

[15] G. Jeschke, DEER distance measurements on proteins, Annu Rev Phys Chem 63 (2012) 419-46.

[16] D. Goldfarb, S. Stoll, Chapter 11, Pulse EPR, EPR spectroscopy. Fundamentals and Methods (Book), John Wiley & Sons, 2018.

[17] D. Goldfarb, S. Stoll, G. Jeschke, Chapter 19, Dipolar Spectroscopy - Double-resonance Methods, EPR spectroscopy. Fundamentals and Methods (Book), John Wiley & Sons, 2018.
[18] S.S. G. Jeschke, DeerAnalysis User Manual - Version 2019, (2019).
[19] S.G. Worswick, J.A. Spencer, G. Jeschke, I. Kuprov, Deep neural network processing of DEER data, Science Advances 4(8) eaat5218.
[20] J. Keeley, T. Choudhury, L. Galazzo, E. Bordignon, A. Feintuch, D. Goldfarb, H. Russell, M.J. Taylor, J.E. Lovett, A. Eggeling, L. Fábregas Ibáñez, K. Keller, M. Yulikov, G. Jeschke, I. Kuprov, Neural networks in pulsed dipolar spectroscopy: A practical guide, Journal of Magnetic Resonance 338 (2022) 107186.
[21] T. von Hagens, Y. Polyhach, M. Sajid, A. Godt, G. Jeschke, Suppression of ghost distances in multiple-spin double electron-electron resonance, Phys Chem Chem Phys 15(16) (2013) 5854-66.
[22] D.M. Bela E. Bode , Jorn Plackmeyer , Gerd Durner, Thomas F. Prisner, Olav Schiemann, Counting the monomers in nanometer-sized oligomers by pulsed electron-electron double resonance, JACS 129 (2007) 6736-6745.
[23] A. Villar-Piqué, T. Lopes da Fonseca, T.F. Outeiro, Structure, function and toxicity of alpha-synuclein: the Bermuda triangle in synucleinopathies, Journal of Neurochemistry 139(S1) (2016) 240-255.
[24] M.u. Rahman, M.W. Ullah, J.A. Shah, S. Sethupathy, H. Bilal, S.A. Abdikakharovich, A.U. Khan, K.A. Khan, N. Elboughdiri, D. Zhu, Harnessing the power of bacterial laccases for xenobiotic degradation in water: A 10-year overview, Science of The Total Environment 918 (2024) 170498.